Thermodynamics of Atomic Clusters Using Variational Quantum Hydrodynamics[†]

Sean W. Derrickson and Eric R. Bittner*

Department of Chemistry and Center for Materials Chemistry, University of Houston, Houston, Texas 77204

Received: March 21, 2007; In Final Form: May 30, 2007

Small clusters of rare-gas atoms are ideal test cases for studying how quantum delocalization affects both the thermodynamics and the structure of molecular scale systems. In this paper, we use a variational quantum hydrodynamic approach to examine the structure and dynamics of $(Ne)_n$ clusters, with n up to 100 atoms, at both $T = 0$ K and for temperatures spanning the solid-to-liquid transition in bulk Ne. Finite temperature contributions are introduced to the grand potential in the form of an "entropy" potential. One surprising result is the prediction of a negative heat capacity for very small clusters that we attribute to the nonadditive nature of the total free-energy for very small systems.

I. Introduction

Rare-gas clusters approximated by the simple Lennard−Jones (LJ) pairwise potential are ideal test cases for many-body simulations,[1−3] providing a useful benchmark for new methods. In addition, rare-gas clusters are often used to probe the transition from microscopic to macroscopic properties in atomic systems. This regime has many unique properties[4] and has been studied with a wide variety of theoretical and experimental techniques.[5−8]

In many-body systems, quantum mechanical effects become important when the de Broglie wavelength of a given atom becomes comparable to the characteristic interatomic interaction length (σ). If we define a characteristic temperature as $T^* = \epsilon/k_B$ in terms of the well-depth, ϵ, one arrives at the de Boer ratio.[9]

$$\Lambda = \frac{\lambda(T^*)}{\sigma} = \frac{\hbar}{\sigma\sqrt{m\epsilon}} \tag{1}$$

In the strictly classical limit, $\Lambda = 0$ whereas systems with $\Lambda > 0.3$ should be considered as strongly quantum mechanical. For example, the de Boer ratio for Ar clusters $\Lambda_{Ar} \approx 0.03$. As such, quantum effects in Ar clusters and liquids play an insignificant role. However, for Ne, $\Lambda_{Ne} \approx 0.1$, and quantum mechanical effects may be important at low temperatures.

In this paper, we extend the quantum hydrodynamic method we recently developed[10] to study the nature of quantum effects for atomic cluster systems at finite temperature through the entropic functional given by Mermin.[11] Our approach assumes that the configurational density $n(\mathbf{r}_1, ..., \mathbf{r}_N)$ can be represented with a superposition of statistical approximates, $p(\mathbf{r}_1, ..., \mathbf{r}_N, c_m)$. The algorithm then uses a Bayesian analysis to determine the best statistical approximates given a statistical sampling of the density. It then uses a grid-free hydrodynamic adaptive approach to relax sample points that make up a statistical sampling of the quantum density to the ground-state equilibrium density.

This methodology is similar and complementary to path integral (PI) methods. This is perhaps best seen by comparing the ring polymers of PI-based methods[12] and "particles"

constituting the density of the de Broglie−Bohm procedure outlined herein. The paths in PI methods trace out a path in imaginary time with identical starting and ending points. This gives a collection of ring "atoms" corresponding to each actual atom. In our description, we have a collection of de Broglie−Bohm particles distributed around some initial position with some initial density that constitutes the density at all times, or steps.

In both methods, a collection of particles is propagated with classical-like equations of motion with some interparticle force that is quantum in nature. In PI methods the uncertainty is maintained by spring forces, usually a result of some harmonic approximation. The total path, and hence the number of pseudo particles that must be propagated, is related to the kinetic energy. In a de Broglie−Bohm based method, the uncertainty is maintained by the quantum force that is rigorously derived from the kinetic term in the Hamiltonian. The complementarity arises because at low temperatures the number of particles necessary for PI-based approaches drastically increases. This particular limitation does not exist for the de Broglie−Bohm based approach we have developed.

In what follows, we present a brief overview of the grid-free adaptive hydrodynamic approach for computing the quantum ground-state density for a system of N nuclei introduced earlier, and then we show how it can be extended to finite temperature. We also give a review of the Bayesian analysis used to deduce the best set of m statistical approximates from a statistical sampling of the density. We then show the quantum hydrodynamical scheme used to adapt the sample points toward a minimal energy configuration. We will then present results on clusters of Ne of up to 37 atoms ($N = 37$) for temperatures ranging from 0 to 30 K, which spans the solid-to-liquid transition for bulk Ne ($T_m = 24.56$ K and $T_b = 27.07$ K). In the present work we will demonstrate that quantum effects can indeed be captured with our hydrodynamic method at finite temperature and that quantum effects lead to some thermodynamic behavior for small, symmetric clusters.

II. Theory

A. Zero-Temperature Theory. The Euler−Lagrange equation for the motion of our particles is derived with the help of the hydrodynamic description of quantum mechanics. We begin

---

10346 *J. Phys. Chem. A, Vol. 111, No. 41, 2007*

Derrickson and Bittner

by specifying the full many-body Hamiltonian, and we will follow along similarly to density functional theory (DFT).[13] The potential corresponds to the nuclear motion of a collection of atoms with pairwise interaction potentials.

$$H = -\sum_{i=1}^{N} \frac{1}{2m_i} \nabla_i^2 + \sum_{i\neq j} V(ij) \qquad (2)$$

where the first term is the sum of the kinetic energies of the individual atoms, and the second is the sum of the potential energy contributions. If we denote with $\mathbf{r}_i$ the vector location of atom i with n_i the corresponding atom's density and if $\mathbf{r} = (\mathbf{r}_1, \mathbf{r}_2, ..., \mathbf{r}_N)$, then we will assume that the arbitrary N-body trial density is separable and is given by eq 3.

$$n(\mathbf{r}) = \prod_i n_i(\mathbf{r}_i) \qquad (3)$$

The energy functional corresponding to this density and Hamiltonian is given by eq 4.

$$E[n] = T[n] + \sum_{i\neq j} \int \int n_i(\mathbf{r}_i)n_j(\mathbf{r}_j)V(ij) \, d\mathbf{r}_i \, d\mathbf{r}_j \qquad (4)$$

The kinetic energy operator is separable because we have assumed distinguishability among the constituent atoms. Therefore, the kinetic energy term is the sum of the individual kinetic energy functionals.

$$T[n(1...N)] = \sum_{i=1}^{N} T_i[n_i(\mathbf{r}_i)] \qquad (5)$$

As in electronic structure DFT, evaluating the kinetic energy functionals is problematic because evaluating the quantum kinetic energy is a nonlocal operator and the density is a local function.[13]

If instead we write the quantum wave function in polar form, as in the hydrodynamic formulation of quantum mechanics[14−16] and also in the time-dependent DFT formulation (eq 6),[17,18]

$$\Psi(\mathbf{r}) = \sqrt{n(\mathbf{r})}e^{i\phi(\mathbf{r})} \qquad (6)$$

where $n(\mathbf{r})$ is given by eq 3, then we can arrive at a stationary condition that, if $\vec{\nabla}\phi = 0$, we get eq 7[19]

$$V(1...N) - \sum_i \frac{1}{2m} \frac{1}{\sqrt{n_i(\mathbf{r}_i)}} \nabla_i^2 \sqrt{n_i(\mathbf{r}_i)} = \text{const} \qquad (7)$$

at all points in space. The constant is the energy of the system. We note here the similarity of the second term in the previous equation with the quantum force from diffusion Monte Carlo ($\vec{\nabla}\psi/\psi$). This term is also known as the quantum potential in the de Broglie−Bohm formulation. By inspection, then, we can define our kinetic energy functional as eq 8.

$$T[n(\mathbf{r}_i)] = -\frac{1}{2m} \int \sqrt{n_i(\mathbf{r}_i)} \nabla_i^2 \sqrt{n_i(\mathbf{r}_i)} \, d\mathbf{r}_i \qquad (8)$$

Integrating by parts and taking $n(i) \rightarrow 0$ at $\pm\infty$ produces the familiar von Weizsacker kinetic energy functional[20] (eq 9).

$$T_W[n(\mathbf{r}_i)] = +\frac{1}{8m} \int \frac{1}{n_i(\mathbf{r}_i)} \vec{\nabla}_i n_i(\mathbf{r}_i) \cdot \vec{\nabla}_i n_i(\mathbf{r}_i) \, d\mathbf{r}_i \qquad (9)$$

Thus, the total energy functional is given in terms of the single particle densities.

$$E[n] = \sum_{i=1}^{N} T_W[n_i(\mathbf{r}_i)] + \sum_{i\neq j} \int \int n_i(\mathbf{r}_i)n_i(\mathbf{r}_j)V(ij) \, d\mathbf{r}_i \, d\mathbf{r}_j \qquad (10)$$

Taking the variation of $E[n]$ with respect to the single-particle densities with the constraint that $\sum_i \int n_i(\mathbf{r}_i) \, d\mathbf{r}_i = N$, eq 11

$$\delta\{\sum_{i=1}^{N} (T_W[n_i(\mathbf{r}_i)] + \sum_{j\neq i} \int \int n_i(\mathbf{r}_i)n_j(\mathbf{r}_j)V(ij) \, d\mathbf{r}_i \, d\mathbf{r}_j - \\ \mu(\int n_i(\mathbf{r}_i) \, d\mathbf{r}_i - 1))\} = 0 \qquad (11)$$

leads to the Euler−Lagrange equation shown in eq 12.

$$\frac{\delta T_W[n_i(\mathbf{r}_i)]}{\delta n_i(\mathbf{r}_i)} + \sum_{j\neq i} \int V(ij)n_j(\mathbf{r}_j) \, d\mathbf{r}_j - \mu = 0 \qquad (12)$$

When satisfied, μ is the vibrational ground-state energy, and the $n_i(\mathbf{r}_i)$ terms are the probability densities of the individual nuclei. This leads to an effective mean-field potential for each atom of the form shown in eq 13.

$$V_i^e = Q(\mathbf{r}_i) + V_e(\mathbf{r}_i) + \sum_{j=1}^{N} V_p(\mathbf{r}_i,\mathbf{r}_j) \qquad (13)$$

Here, $Q(\mathbf{r})$ is the quantum potential, $V_e(\mathbf{r}_i)$ is an external potential that corresponds to any external driving field ($V_e = 0$ in the present study), and $V_p(\mathbf{r}_i, \mathbf{r}_j)$ is the pairwise interatomic interaction potential.

B. Finite Temperature. For a system at finite temperature under the conditions of a grand ensemble, $Z(T, V, \mu) = Tr\{e^{-\beta(H-\mu N)}\}$, an equilibrium state density matrix will minimize Ω, the grand potential. This is given by eq 14,

$$\Omega = -\frac{1}{\beta} \ln(Tr\{e^{-\beta(H-\mu N)}\}) \qquad (14)$$

where H is the Hamiltonian, N is the number operator, and μ is the chemical potential. Nearly 40 years ago, Mermin[11] showed that by writing Ω as a functional of an arbitrary trial density matrix (eq 15)

$$\Omega[\hat{\rho}_T] = Tr\left\{\hat{\rho}_T\left(K + V - \mu N + \frac{1}{\beta} \ln \hat{\rho}_T\right)\right\} \qquad (15)$$

$\delta\Omega = 0$ only if the correct density matrix is used. Thus, for any trial density matrix $\hat{\rho}_T \neq \hat{\rho}$, then $\Omega[\hat{\rho}_T] \geq \Omega[\hat{\rho}]$. Mermin also shows that there is a unique density associated with the equilibrium density matrix, $n(\mathbf{r}) = Tr\{\hat{\rho}|\psi(\mathbf{r})|^2\}$. This implies that one can write the grand potential as a functional of the density (eq 16)

$$\Omega[n(\mathbf{r})] = F[n(\mathbf{r})] - \mu \int n(\mathbf{r}) \, d\mathbf{r} \qquad (16)$$

where our free-energy functional $F[n]$ is given by eq 17.

$$F[n(\mathbf{r})] = Tr\left\{\hat{\rho}[n(\mathbf{r})]\left(K + V + \frac{1}{\beta} \ln \hat{\rho}[n(\mathbf{r})]\right)\right\} = \\ T_W[n(\mathbf{r})] + V[n(\mathbf{r})] + \frac{1}{\beta} S[n(\mathbf{r})] \qquad (17)$$

Here we have made the substitution of $S[n(\mathbf{r})]$ for the entropic term. The T_W functional is the Weizsacker functional that, along

Thermodynamics of Atomic Clusters

J. Phys. Chem. A, Vol. 111, No. 41, 2007 **10347**

with the potential functional, is identical to our previous work[10] as well as section IIA. We have excluded exchange and correlation terms because we have assumed noninteracting particles. The inverse temperature (β) is a Lagrange multiplier used in the determination of the ground-state density. This is similar to the chemical potential used previously in the determination of the ground-state at $T = 0$. The minimum of the Ω functional will correspond to the atomic density profile of the system at a given temperature. Note that the free-energy functional, $F[n]$, contains the kinetic energy and external potential operators as well as an entropy/temperature term, so that now the stationary equilibrium state will now be an energetic compromise between the quantum and the entropic potentials, both of which tend to destabilize the clusters, and a mean-field interaction potential that tends to stabilize the clusters. The net effect is that as the cluster temperature increases the clusters will be increasingly unstable and undergo transitions from ordered to disordered states.

The thermodynamic justification for the form of the entropic functional defined by Mermin can be seen from the form of the entropy in Boltzmann's eulogistic equation (eq 18);

$$S = k_B \ln(\Omega_{mc}) \tag{18}$$

where Ω_{mc} is the microcanonical density of states. Because we can write Ω_{mc} in terms of the density matrix in the von Neumann definition of entropy, we can write the above equation as eq 19.

$$S = -k_B Tr\{\hat{\rho}[n(\mathbf{r})] \ln(\hat{\rho}[n(\mathbf{r})])\} \tag{19}$$

This is also sometimes called the differential entropy. The entropic functional takes into account the contribution from temperature-entropy work into our energy functional.

We can minimize Ω to obtain the chemical potential (eq 20).

$$\mu = \frac{1}{\beta}\frac{\delta S[n]}{\delta n(\mathbf{r})} + Q(\mathbf{r}) + V_{ext}(\mathbf{r}) \tag{20}$$

Again, Q is the quantum potential derived from the functional derivative of the Weizsacker term, $Q = \delta T[n]/\delta n$, and in a similar manner, V_{ext} is simply the mean-field potential of a given atom in terms of all the other atoms. Now all that remains is to calculate this iteratively, as in our previous work,[10] with a temperature correction related to $S[n(\mathbf{r})]$.

We assume that the entropic contribution is additive and can be derived using the von Neumann entropy (eq 21);

$$S[n(\mathbf{r})] = \frac{1}{\beta}\sum_i \int n_i(\mathbf{r}_i) \ln(n_i(\mathbf{r}_i)) \, d\mathbf{r}_i = \sum_i S[n(i)] \tag{21}$$

where the sum is over individual atoms. Taking the functional derivative with respect to the density, needed in the equations of motion of the particles, we define an "entropic force" as eq 22.

$$\frac{\delta S[n(\mathbf{r})]}{\delta n_i} = \frac{1}{\beta}(\ln(n_i(\mathbf{r}_i)) + 1) \tag{22}$$

To test our assumption and verify its range of applicability, we consider a simple harmonic system with a normalized Gaussian density function (eq 23).

$$n(x) = \sqrt{\frac{1}{2\pi\langle x^2 \rangle}} e^{-x^2/2\langle x^2 \rangle} \tag{23}$$

As such, the free-energy (with $\hbar = 1$) is given by eq 24.

$$\langle F \rangle = \frac{1}{8m\langle x^2 \rangle} + \frac{m\omega^2}{2}\langle x^2 \rangle - \frac{1}{2\beta}(\ln(2\pi\langle x^2 \rangle) + 1) \tag{24}$$

The first two terms are simply the average kinetic and potential energies. The last term is temperature dependent and arises from the entropy contribution. Minimizing $\langle F \rangle$ with respect to $\langle x^2 \rangle$ yields an optimal width parameter given by eq 25.

$$\langle x^2 \rangle_{opt} = \frac{k_B T}{2m\omega^2}(1 + \sqrt{1 + (\hbar\omega/k_B T)^2}) \tag{25}$$

For comparison, the exact expression for the width of a harmonic oscillator at finite temperature is[21] given by eq 26;

$$\langle x^2 \rangle_{exact} = \frac{\hbar}{2m\omega} \coth\left(\frac{\Theta_v}{2T}\right) \tag{26}$$

where $\Theta_v = \hbar\omega/k_B$ is the vibrational temperature. In Figure 1 we compare the Mermin functional versus the exact result for a system with $\hbar/m\omega = 1$. Clearly, the delocalization obtained using the Mermin functional approaches the exact result asymptotically at high temperatures. It also agrees perfectly at $T = 0$. However, for intermediate temperatures, $T \lesssim 2\Theta_v$, $\langle x^2 \rangle_{approx} > \langle x^2 \rangle_{exact}$. Consequently, we anticipate that the Mermin approximation to the entropy functional will systematically overestimate quantum delocalization effects for $T < \Theta_v$. This indicates that a corrected form for the entropic potential is necessary.

1. Computational Approach: Mixture Model. To utilize the hydrodynamic description, one needs a quantitative description of the density. This will be done directly from an ensemble of points sampled from the initial quantum density in the following way. To begin, the single-particle probability distribution functions (PDF) can be represented by a mixture model[22,23] by summing a finite number M of density approximates by eq 27;

$$n(\mathbf{r}) = \sum_m^M p(\mathbf{r}, c_m) \tag{27}$$

where $p(\mathbf{r}, c_m)$ is the probability that a randomly chosen member of the ensemble has the configuration $\mathbf{r}$ and is a variant of the mth approximate designated by c_m. These approximates may be Gaussians or any other integrable multidimensional function that can be parametrized by its moments. For Gaussian clusters, we have a weight $p(c_m)$, a mean position vector μ_m, and a covariance matrix C_m.

By definition, each joint probability in eq 27 is related to a pair of conditional probabilities according to the relation shown in eq 28.

$$p(\mathbf{r}, c_m) = p(c_m)p(\mathbf{r}|c_m) = n(\mathbf{r})p(c_m|\mathbf{r}) \tag{28}$$

The forward conditional probability $p(\mathbf{r}|c_m)$ refers to the probability that a randomly chosen variant of c_m has the configuration $\mathbf{r}$, and the posterior probability $p(c_m|\mathbf{r})$ refers to the probability that the configuration point r is a variant of the approximate c_m. Note that $n(\mathbf{r})$ and $p(c_m)$ are the quantum density and weight of the mth approximate, respectively.

As shown in our previous works,[10,24] this formulation can be used to define a multidimensional quantum density with user defined amounts of correlation between the particles. Briefly, we outline our procedure as follows.
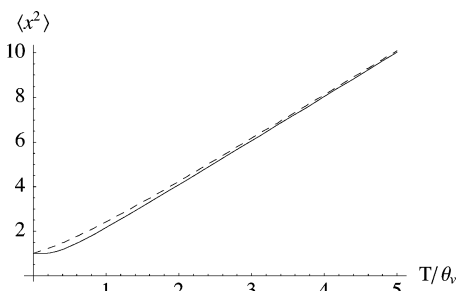
Figure 1. $\langle x^2 \rangle$ vs T, comparing the approximate entropy functional of eq 21 (---) to the exact (—) value for a harmonic system at finite temperature.

With a Gaussian model representing the full $3N$ dimensional system,

$$p(\mathbf{r}|c_m) = \sqrt{\frac{||\mathbf{C}^{-1}||}{(2\pi)^{N_d}}} \, e^{(\mathbf{r}_d - \mu_{m,d})\mathbf{C}_m^{-1}(\mathbf{r}_d - \mu_{m,d})} \qquad (29)$$

where the covariance matrix ($\mathbf{C}$), eq 29 can be used to eliminate (or maintain) coupling between various degrees of freedom. We note that for the present work the elements of $\mathbf{C}$, which provide coupling between atoms or degrees of freedom, are set to zero. This means that correlations are only taken into account within each atom.

One must determine the Gaussian parameters $p(c_m)$, μ_m, and C_m, that define the density. This is facilitated by using an iterative expectation maximization (EM) algorithm. In each case, these are readily approximated by summing over an ensemble of points $\{\mathbf{r}_n\}$ sampled from the $n(\mathbf{r})$ or PDF. For instance, the mean positions are approximated with eq 30.

$$\mu_m \approx \frac{1}{Np(c_m)} \sum_n^N \mathbf{r}_n p(c_m|\mathbf{r}_n) \qquad (30)$$

The updated Gaussian parameters are then used to update the posterior terms $p(c_m|\mathbf{r}_n)$ for each $\mathbf{r}_n$ sample point by inserting this back into eq 29 and using Bayes' equation (eq 31).

$$p(c_m|\mathbf{r}_n) = \frac{p(c_m)p(\mathbf{r}_n|c_m)}{\sum_m p(c_m)p(\mathbf{r}_n|c_m)} \qquad (31)$$

This procedure progressively solves for the best set of parameters given a distribution of sample points.

The expectation maximization algorithm described above allows us to generate an approximate analytical functional form for the single-particle density via statistical sampling over an ensemble of points. The next step is to adjust the single-particle densities themselves to produce a lower total energy. We do this by deriving the quantum hydrodynamic equations of motion for the sample points, $\mathbf{r}_{in}$, where i labels a given atom and n labels a given sample point associated with density $n_i(\mathbf{r})$.

2. Computational Approach: Equations of Motion for the Sample Points. The quantum Hamilton–Jacobi equation generates the equations of motion for the ray-lines of a time-dependent solution to the Schrödinger equation.[25–28] This allows convergence to the ground-state by relaxing along an action field determined for each atom. This gives a set of time-dependent self-consistent field equations whereby the motion of atom i is determined by the average potential

interaction between atom i and the rest of the atoms in the system.

$$\dot{S}_i(\mathbf{r}) + \frac{|\vec{\nabla}_i S|^2}{2m_i} + \sum_{j\neq i} \int V(ij)n_j(\mathbf{r}) \, d\mathbf{r} -$$

$$\frac{1}{2m_i} \frac{1}{\sqrt{n_i(\mathbf{r})}} \nabla_i^2 \sqrt{n_i(\mathbf{r})} + \frac{1}{\beta} n_i(\mathbf{r}) \ln(n_i(\mathbf{r})) = 0 \quad (32)$$

Taking $\vec{\nabla}S = \mathbf{p}$ as a momentum of a particle, the equations of motion along a given ray-line or sample particle $\mathbf{r}_{in}(t)$ of the quantum wave function are given by eq 33;

$$m_i \ddot{\mathbf{r}}_{in} =$$
$$-\sum_{j\neq i} \int (\vec{\nabla}_i V(ij))n(\mathbf{r}_j) \, d\mathbf{r}_j - \vec{\nabla}_i Q[n(\mathbf{r}_i)] + \vec{\nabla}_i \frac{\delta S[n(i)]}{\delta n_i} \quad (33)$$

where $Q[n(i)]$ is the Bohmian quantum potential specified by the last term in eq 32. Stationary solutions of the time-dependent Schrödinger equation are obtained whenever $m_i \ddot{\mathbf{r}}_{in} = 0$. Consequently, we reach the ground-state by relaxing the sample points in a direction along the energy gradient (eq 34),

$$\vec{\nabla}_i E =$$
$$-\sum_{j\neq i} \int (\vec{\nabla}_i V(ij))n_j(\mathbf{r}_j) \, d\mathbf{r}_j - \vec{\nabla}_i Q[n_i(\mathbf{r}_i)] + \vec{\nabla}_i \frac{\delta S[n(i)]}{\delta n_i} \quad (34)$$

keeping $n(\mathbf{r}_j)$ fixed. This generates a new statistical sampling, which we then use to determine a new set of approximates, and the process is repeated.

The algorithm can be summarized by the following steps: (1) For each atom, generate and sample a normalized trial density $n_i(\mathbf{r}_i)$. (2) Using the EM routines and the given sample of points, compute the coefficients for the density approximates. (3) Compute the forces on each point using eq 32 and advance each point along the energy gradient for one "time" step, either discarding or dampening the velocity of each point. This generates a new sample of points describing the single-particle density for each atom. The new distribution should have a lower total energy because we moved the sample points in the direction toward lower energy.

By iterating through these last two steps, we rapidly converge toward the global quantum energy minimum of the system.

III. Results

A. Zero-Temperature Results. In all the calculations presented here, we used 100 statistical points to represent the density of each atom, and we propagated the SCF equations described above until the energy and the density were sufficiently converged. To reach convergence, this typically required a few hundred thousand iterations. The LJ parameters used for the Ne atoms are $\epsilon = 0.3059$ kJ/mol and $\sigma = 2.79$ Å.[29] The initial centers of the Gaussian approximates correspond to the position of the global energy minima for each clusters with initial widths taken from a harmonic oscillator approximation.

The primary motivation for continuing the study of these clusters at zero-temperature is the desire to be able to accurately simulate bulk systems. In our previous work[10] we were limited to systems with less than 20 atoms. Subsequent improvement of our algorithms have allowed us to substantially advance past this limit. Furthermore, it is recognized that roughly 110 atoms per unit cell are required to reasonably approximate the bulk
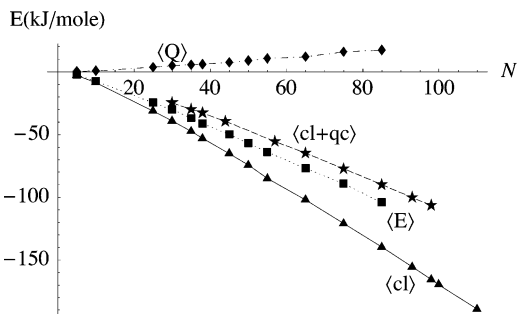
Thermodynamics of Atomic Clusters

J. Phys. Chem. A, Vol. 111, No. 41, 2007 **10349**

Figure 2. Various energetic contributions for quantum and classical Ne clusters vs cluster size, N. Key: $\langle cl \rangle$ = classical global potential minimum energy, $\langle cl+qc \rangle$ = zero-point energy corrections from ref 6, $\langle E \rangle$ = total energy, $\langle Q \rangle$ = quantum kinetic energy (from quantum potential).

TABLE 1: Ground State Vibrational Energies for Ne$_n$ Clusters for Our Results Compared to the Results Tabulated by Calvo et al. in Ref 6

cluster	order	energy (from ref 6)	order	this work
17C	(1)	−11.0853	(2)	−16.6336
17B	(2)	−11.0814	(3)	−16.3188
17A	(3)	−11.0633	(1)	−16.6699
27B	(1)	−21.5483	(2)	−27.6994
27A	(2)	−21.5099	(1)	−28.2823
28B	(1)	−22.5892	(2)	−28.7459
28A	(2)	−22.5496	(1)	−29.3524

behavior of large cluster systems.[30] Even so, our current computational resources limited us to clusters with up to 85 atoms at $T = 0$ K and roughly half this at higher temperatures.

Our $T = 0$ K results are summarized in Figure 2, which shows the various contributions to the total energy. First, we note that the contribution from the quantum potential (average kinetic energy) increases monotonically with system size. Moreover, the total energy $\langle E \rangle$ decreases monotonically. This is to be expected because the larger clusters have increasingly more nearest-neighbor interactions as the size of the system increases.

In Figure 2 we also compare the present results to a similar semiclassical study by Calvo et al.[6] In their results the zero-point energy of the static structure of the global minimum was calculated and then added in an ad hoc fashion to the pair-potential interaction. Generally, our results lie somewhat lower in total energy than the semiclassical estimates but above the classical global energy minimum for each cluster. We do note, however, that the inclusion of the quantum potential alters the total energy surface. Consequently, in some cases, the system could relax to a different minimum or in a superposition of close-lying minima due to tunneling. The clustering model can handle this situation through the inclusion of multiple Gaussian approximates for each atom. However, in each case examined here, we did not observe serious deviations or tunneling between nearly degenerate structures.

However, it is possible that the inclusion of quantum delocalization can influence the energetic ordering of nearly equivalent structures. Calvo et al. also investigated changes in ground-state structure as a result of quantum delocalization. They did this using a basin-hopping Monte Carlo optimization algorithm to explore the energy landscape of small Ne clusters with less than 100 atoms. In this study the zero-point energy contributions were again approximated in an ad hoc fashion similar to that shown in Figure 2. This can be summarized with the following procedure: An initial Monte Carlo search over the potential energy hypersurface is performed to determine a test configuration. The zero-point energy of this test configuration is determined using the static atomic positions. The calculated zero-point energy is then added to the classical potential energy, and this sum is used for the Metropolis acceptance criteria. This process is repeated until the lowest energy configuration is determined, now including both the pair-potential and the zero-point energy.

In our study, as well as that from ref 6, the starting configurations were based upon the global classical minimum on the potential energy hypersurface of the cluster. In Calvo et al.'s semiclassical results, quantum effects produced different global minimum for 35 out of 99 cases for Ne$_n$ in the range of

$n \leq 100$. For example, the 17 atom cluster has three nearly equivalent minima (17A, 17B, and 17C) with energies $E_C < E_B < E_A$ separated by substantial potential barriers; likewise, $n = 27$ and $n = 28$ each have two energetically similar minima. The energies (from ref 6) of these are given in Table 1. Remarkably, our results show a different ordering of the energies of these structures compared to the semiclassical results. The difference between the two results is consistent with the general trend shown in Figure 2 and corresponds to the different levels of theory used in each study. In the semiclassical approach, zero-point contributions are estimated from the curvature of the potential, after energy "relaxation" on the potential energy hypersurface. However, in our approach the quantum delocalization self-consistently alters the $3N$-dimensional total energy hypersurface being sampled.

B. Finite Temperature Results. The thermodynamics of small molecular scale systems is of considerable interest because what are typically extensive variables (e.g., total energy, entropy, etc.) that scale monotonically with system size can exhibit anomalous behavior as the system size becomes small. Add to this the influences of quantum delocalization, and one anticipates the predicted thermodynamics of these system to exhibit behavior quite different from the bulk or even from a purely classical prediction.

One attractive way to introduce quantum corrections into an otherwise classical molecular dynamics or Monte Carlo simulation is through the use of an effective "quantum potential". Typically, such effective potentials are expansions of the quantum partition function in powers of $\hbar$. The Feynman−Hibbs potential is derived by characterizing a quantum particle with a Gaussian that has a width equal to the thermal de Broglie length centered about the particle and accounts for the spread in density expected for quantum particles. Under these assumptions the partition function can be simplified, and with a Gaussian density the pair-potential term would be evaluated with eq 35

$$V(\mathbf{r}_{ij}) = \left(\frac{2\mu}{\pi\beta\hbar^2}\right)^{3/2} \int dR V(|r + R|)e^{-2\mu/\beta\hbar^2 R^2} \quad (35)$$

with some reduced mass, μ. The effective potential can then be found by expanding about r and truncating at some convenient order. Calvo et al.[6] performed similar calculations using eq 36

$$V_{\text{eff}}(r) = V(r) + \frac{\hbar^2\beta}{24m} V''(r) \quad (36)$$

in a very comprehensive survey of how quantum delocalization affects the structure and energetics of rare-gas clusters, and as such provides a highly useful point of comparison for our approach. We do note that these expansions assume λ to be small (compared to the local variation in the potential), as per the semiclassical WKB criteria. Consequently, for lower temperatures and higher degrees of quantum delocalization, such effective quantum corrections are not applicable.

Here we focus on three clusters (Ne_{13}, Ne_{17}, and Ne_{37}) over a temperature range spanning the solid-to-liquid transition for bulk Ne. In the figures, which display the thermodynamic data, the temperature is given in reduced units, which is the temperature in Kelvin multiplied by Boltzmann's constant and divided by the well depth of the LJ potential, $T' = Tk_B/\epsilon$. Figure 3 shows the total free-energy (scaled to a common $T = 0$ K origin) versus temperature for the three clusters. Figure 4 shows the various contributions to the total free-energy for the 13 atom cluster with similar behavior for the other clusters. First, the contribution from the quantum potential increases as T increases, as it should. The averaged quantum potential is simply the average quantum kinetic energy and, as such, is approximately inversely proportional to the de Broglie wavelength squared, $\langle Q \rangle \propto \lambda^{-2}$. Hence, $\langle Q \rangle$ increases as the system becomes more localized, corresponding to an increasingly shorter thermal de Broglie wavelength as T increases.

At higher temperatures, though, the quantum effects will be washed out as the de Broglie wavelength goes to zero. So, we expect that these factors will only be apparent at lower temperatures. The de Broglie wavelength decreases because the entropic potential causes an increase in the effective well depth that the atom feels with increasing T. As this happens, the cohesive forces increase in response to the decreased delocalization. This is a counterintuitive result because the cohesive forces are expected to decrease at higher temperatures. This results from the ability of atomic clusters to preferentially store energy in the internal interaction energy rather than kinetic. This aspect is discussed later.

It is useful to compare the results we have obtained with the analytical results obtained using the Debye model, which is known to have the correct low temperature behavior for the heat capacity in the bulk material. The Debye model has a single adjustable parameter, the Debye temperature, defined by eq 37;

$$T_D = \frac{hc_s}{2k_B}\left(\frac{6N}{\pi V}\right)^{-3} \tag{37}$$

where $N/V = \rho$ is the bulk density, and c_s is the speed of sound in the medium. From this we can derive the internal energy as eq 38.

$$U = 9Nk_B T(T/T_D)^3 \int_0^{T_D/T} \frac{x^3}{e^x - 1}\, dx \tag{38}$$

In general, T_D is determined by fitting the model to experimental thermodynamic data. For bulk Ne, $T_D = 75$ K.

Figure 5 compares the internal energy from our results to the Debye model, with the Debye energy shifted so that it corresponds at $T = 0$ K with our results. By comparing the curves it is evident our results for the 17 and 37 atom systems will give similar Debye temperatures to the bulk limit. The melting region can be identified as the nonlinear regions of the internal energy curves. In all three clusters, similar melting regions are observed for both approaches. It may seem remarkable that the Debye model is still useful given the fact that these clusters are far from the bulk limit. However, the Debye model was constructed to account for both the high- and low-temperature caloric curves in condensed phase systems, and there is no fundamental problem with it as an approximation in this case.

Closer inspection of the internal energy curve for Ne_{13} indicates that, for temperatures $0 < T \leq 0.2T'$, the internal energy decreases to some extent. This corresponds to a negative
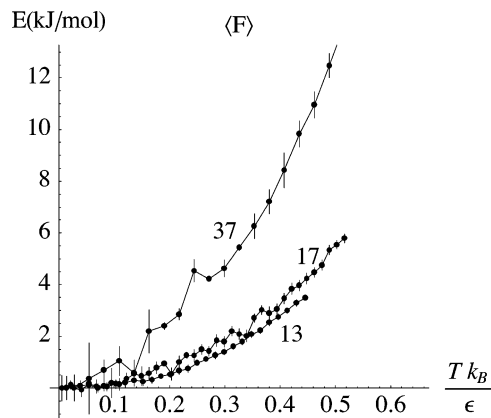

Figure 3. The free-energy of the different clusters vs T. Error bars indicate numerical/statistical precision of each computed free-energy value. Note the $T = 0$ values are offset to a common origin for comparison. The energies at $T = 0$ K for the three clusters are as follows: $F_0^{13} = -11.21$ kJ/mol, $F_0^{17} = -15.216$ kJ/mol, and $F_0^{37} = -39.03$ kJ/mol.

heat capacity. Even given a computational error estimate of ± 0.1 kJ/mol in the internal energy, the dip is clearly present in our results. This is not entirely unreasonable or unprecedented as several recent studies have predicted negative heat capacities for atomic clusters;[4-6] however, in ref 6 this was dismissed as an unphysical result. In addition, negative heat capacities have also been observed recently for sodium clusters of 147 atoms.[31] Schmidt et al.[31] explain this for small atomic systems as a purely microscopic phenomenon. That is, for larger systems at a phase transition, energy is added as potential energy rather than kinetic energy so that the temperature remains constant over the course of the transition. For molecular scale atomic systems, on the other hand, it can be entropically favorable to avoid a partially melted state so that some energy is actually transferred from kinetic to potential energy, causing a negative heat capacity near phase transitions. Negative heat capacities are not predicted by the Debye model, indicating that anharmonic delocalization effects may be important for describing negative heat capacities. Another factor is that $N = 13$ and 147 clusters form complete icosohedral structures in their lowest energy state. These are called magic number clusters because of the stability of these highly symmetric forms. Because negative heat capacities have only been observed and/or predicted for magic number clusters, this suggests that the negative heat capacity may be related to the symmetry of these systems.

It is also interesting to note that negative heat capacities have been predicted in astronomical systems for some time.[32] This had a very simple justification based around a viral analysis for a $1/r$-potential system. This was met with some reluctance in the physics community, of course, but it has become established based upon some recent examples.[33] In all instances of negative heat capacity the common factor is that the energy is not an extensive quantity and the interactions between subsystems must be taken into account. In the clusters we are examining, as the temperature is raised the atoms adjust themselves to store energy in the pair-potential interaction between atoms rather than increase the kinetic energy. This process can result in a negative heat capacity.

On the basis of the above discussions, we can say the thermodynamics of these clusters is influenced greatly by their relative ability to store energy preferentially as potential energy. This aspect of these systems can be studied by introducing a virial-like parameter consisting of the ratio of the quantum potential with the total internal energy, $\langle Q \rangle \langle U \rangle$. This parameter
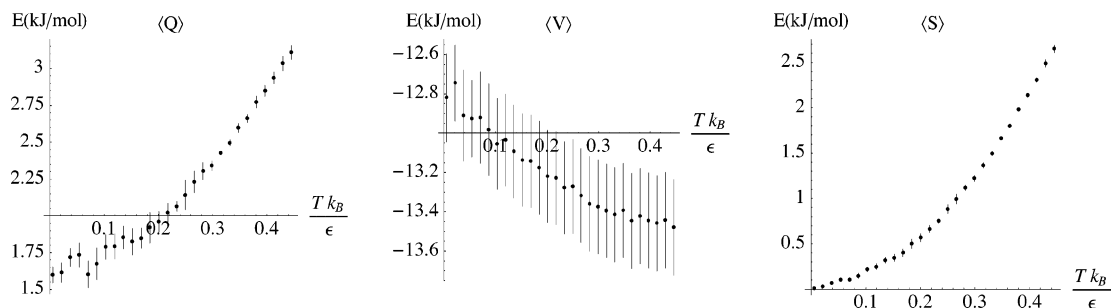
Thermodynamics of Atomic Clusters

J. Phys. Chem. A, Vol. 111, No. 41, 2007 **10351**

Figure 4. Plots of the quantum, total potential, and entropic contributions to the total free-energy vs T for Ne$_{13}$.
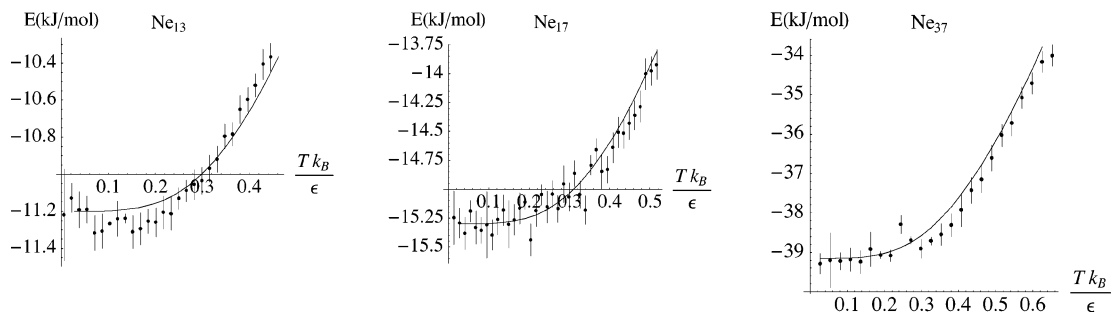

Figure 5. Internal energy comparison of the current results, with error bars, with the Debye model (−).
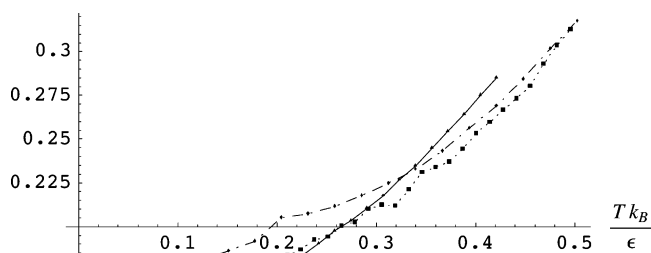

Figure 6. $(\langle Q \rangle / \langle U \rangle)$ vs T. (Key: −, 13 atoms; ···,17 atoms; − · −, 37 atoms).

essentially measures the percentage of energy contained in the kinetic energy. This will be given by the following equation.

$$\tau_m = -\frac{\langle Q \rangle}{\langle Q \rangle + \langle V \rangle}$$

The value of τ_m should approach 1 as the temperature is raised because the averaged quantum potential value increases with temperature, and the averaged potential interaction energy should remain about constant, although the cluster will dissociate into a disordered state long before this point is reached. The averaged quantum potential value is a monotonically increasing function of the temperature because it is inversely proportional to the delocalization, or the de Broglie wavelength, $\langle Q \rangle \approx 1/\lambda^2 \approx T$. The value of τ_m is shown for the three clusters in Figure 6, and the curves clearly show that the smaller clusters must increase the amount of kinetic energy at a greater rate with temperature. Essentially, the different rates of increase for τ_m are due to the larger clusters increased ability to store energy in the pair-potential. This explains the marked decrease in the temperatures of phase transitions as the size of the clusters drops.

IV. Conclusions

In this work, we have investigated the ground vibrational state energies at zero-temperature and the low temperature thermo-dynamics of rare-gas clusters. The method used is a novel approach we previously developed based upon an "orbital" free DFT. It also utilizes the Bohm hydrodynamical description of quantum mechanics similar to time dependent DFT, and an information theoretical approach is used to determine an optimal quantum density function. Improvements in the algorithm allowed the calculation of the ground-state structure at zero-temperature approaching the size necessary to simulate bulk systems.

We have also outlined the theoretical development necessary for the calculation of the ground-state vibrational energy at low temperatures. This involves the introduction of an "entropic" potential which resembles the von Nuemann definition of the entropy. This approach was tested by measuring the thermo-dynamic behavior for temperatures spanning the quasiphase transition of atomic clusters under 40 atoms. Results indicate excellent agreement with previous studies. Good agreement is also seen with the analytical results from the Debye model, which is surprisingly accurate even when far from the bulk or continuum limit.

The zero-temperature results indicate that the level of theory used in the calculation of quantum effects can influence the ground-state structures that are calculated. This could have major implications for some global optimization methods. We also presented a virial-like parameter to help illustrate the melting characteristics of these clusters. This melting parameter shows that the reason for the significantly lower temperatures for phase transitions in microscopic clusters is their decreased ability to store energy in the total pair-potential energy. The most striking aspect of the present results is the negative heat capacity seen for Ne$_{13}$. This has only been predicted or observed for so-called magic number clusters, which implies that it is symmetry related. In this work, we have shown that our approach is useful for accurately predicting ground-state energies and thermodynamics for atomic clusters influenced by quantum delocalization.

Foundation and the Robert Welch Foundation as well as the TLC^2 at the University of Houston.

References and Notes

(1) Berry, R. S. *Phys. J. Chem.* **1994**, *98*, 6910.

(2) Lynden-Bell, R. M.; Wales, D. J. *J. Chem. Phys.* **1994**, *101*, 1460.

(3) Predescu, C.; Frantsuzov, P. A.; Mandelshtam, V. A. *J. Chem. Phys.* **2005** (122), 154305.

(4) Bixon, M.; Jortner, J. *J. Chem. Phys.* **1989**, *91*, 1631.

(5) Labastie, P.; Whetten, R. L. *Phys. Rev. Lett.* **1990**, *65*, 1567.

(6) Calvo, F.; Doye, J. P. K.; Wales, D. J. *J. Chem. Phys.* **2001**, *114*, 7312.

(7) Beck, T. L.; Berry, R. S. *J. Chem. Phys.* **1988**, *88*, 3910.

(8) Jellinek, J.; Beck, T. L.; Berry, R. S. *J. Chem. Phys.* **1986**, *84*, 2783.

(9) Toda, R. K. M.; Saito, N. *Statistical Physics I: Equilibrium Statistical Mechanics*; Berlin: Springer, 1992.

(10) Derrickson, S.; Bittner, E. *J.Phys. Chem. A* **2006**, *110*, 5333.

(11) Mermin, N. D. *Phys. Rev.* **1965**, *137*, A1441.

(12) Chandler, D.; Wolynes, P. G. *J. Chem. Phys.* **1981**, *74*, 4078.

(13) Parr, R. G.; Yang, W. *Density Functional Theory of Atoms and Molecules*; Clarendon Press: New York, 1989.

(14) Madelung, E. *Phys. Z.* **1926**, *40*, 322.

(15) de Broglie, L. *C. R. Acad. Sci. Paris* **1926**, *183*, 447.

(16) de Broglie, L. *C. R. Acad. Sci. Paris* **1927**, *184*, 273.

(17) Banerjee, A.; Harbola, M. K. *J. Chem. Phys.* **2000**, *113*, 5614.

(18) Banerjee, A.; Harbola, M. K. *J. Chem. Phys.* **2002**, *117*, 7845.

(19) Holland, P. R. *The Quantum Theory of Motion*; Cambridge University Press: New York, 1993.

(20) von Weizsacker, C. F. *Phys. Z.* **1935**, *96*, 431.

(21) Feynman, R. P. *Statistical Mechanics: A Set of Lectures*; Addison−Wesley Publishing Company, Inc.: Boston, 1972.

(22) Gershenfeld, N. *The Nature of Mathematical Modeling*; Cambridge University Press: Cambridge, U.K., 1999.

(23) McLachlan, G. J.; Basford, K. E. *Mixture models: Inference and Applications to Clustering*; Dekker, Inc.: New York, 1988 and 1998.

(24) Maddox, J. B.; Bittner, E. R. *J. Chem. Phys.* **2003**, *119*, 6465.

(25) Bohm, D. *Phys. Rev.* **1952**, *85*, 166.

(26) Bohm, D. *Phys. Rev.* **1952**, *85*, 180.

(27) Bohm, D.; Hiley, B. J.; Kaloyerou, P. N. *Phys. Rep.* **1987**, *144*, 321.

(28) Wyatt, R. E. *Chem. Phys. Lett.* **1999**, *313*, 189.

(29) Livesly, D. M.; *J. Phys. C: Solid State Phys.* **1983**, *16*, 2889.

(30) Solca, J.; Dyson, A. J.; Steinebrunner, G.; Kirchner, B.; Huber, H. *J. Chem. Phys.* **1998**, *108*, 4107.

(31) Schmidt, M.; Kusche, R.; Hippler, T.; Donges, J.; Kronmüller, W.; von Issendorff, B.; Haberland, H. *Phys. Rev. Lett.* **2001**, *86*, 1191.

(32) Lynden-Bell, D. *Physica A* **1999**, *263*, 293.

(33) Posch, H. A.; Thirring, W. *Phys. Rev. Lett.* 2005, *95*, 251101.